

University of Groningen

Favorable Mixing Thermodynamics in Ternary Polymer Blends for Realizing High Efficiency Plastic Solar Cells

Gasparini, Nicola; Kahmann, Simon; Salvador, Michael; Perea, Jose Dario; Sperlich, Andreas; Baumann, Andreas; Li, Ning; Rechberger, Stefanie; Spiecker, Erdmann; Dyakonov, Vladimir

Published in:
Advanced Energy Materials

DOI:
[10.1002/aenm.201803394](https://doi.org/10.1002/aenm.201803394)

IMPORTANT NOTE: You are advised to consult the publisher's version (publisher's PDF) if you wish to cite from it. Please check the document version below.

Document Version
Publisher's PDF, also known as Version of record

Publication date:
2019

[Link to publication in University of Groningen/UMCG research database](#)

Citation for published version (APA):

Gasparini, N., Kahmann, S., Salvador, M., Perea, J. D., Sperlich, A., Baumann, A., Li, N., Rechberger, S., Spiecker, E., Dyakonov, V., Portale, G., Loi, M. A., Brabec, C. J., & Ameri, T. (2019). Favorable Mixing Thermodynamics in Ternary Polymer Blends for Realizing High Efficiency Plastic Solar Cells. *Advanced Energy Materials*, 9(19), [1803394]. <https://doi.org/10.1002/aenm.201803394>

Copyright

Other than for strictly personal use, it is not permitted to download or to forward/distribute the text or part of it without the consent of the author(s) and/or copyright holder(s), unless the work is under an open content license (like Creative Commons).

The publication may also be distributed here under the terms of Article 25fa of the Dutch Copyright Act, indicated by the "Taverne" license. More information can be found on the University of Groningen website: <https://www.rug.nl/library/open-access/self-archiving-pure/taverne-amendment>.

Take-down policy

If you believe that this document breaches copyright please contact us providing details, and we will remove access to the work immediately and investigate your claim.

Favorable Mixing Thermodynamics in Ternary Polymer Blends for Realizing High Efficiency Plastic Solar Cells

Nicola Gasparini,* Simon Kahmann, Michael Salvador, Jose Dario Perea, Andreas Sperlich, Andreas Baumann, Ning Li, Stefanie Rechberger, Erdmann Spiecker, Vladimir Dyakonov, Giuseppe Portale, Maria A. Loi, Christoph J. Brabec,* and Tayebbeh Ameri*

Ternary blends with broad spectral absorption have the potential to increase charge generation in organic solar cells but feature additional complexity due to limited intermixing and electronic mismatch. Here, a model system comprising the polymers poly[5,5-bis(2-butyloctyl)-(2,2-bithiophene)-4,4-dicarboxylate-alt-5,5-2,2-bithiophene] (PDCBT) and PTB7-Th and PC₇₀BM as an electron accepting unit is presented. The power conversion efficiency (PCE) of the ternary system clearly surpasses the performance of either of the binary systems. The photophysics is governed by a fast energy transfer process from PDCBT to PTB7-Th, followed by electron transfer at the PTB7-Th:fullerene interface. The morphological motif in the ternary blend is characterized by polymer fibers. Based on a combination of photophysical analysis, GIWAXS measurements and calculation of the intermolecular parameter, the latter indicating a very favorable molecular affinity between PDCBT and PTB7-Th, it is proposed that an efficient charge generation mechanism is possible because PTB7-Th predominantly orients around PDCBT filaments, allowing energy to be effectively relayed from PDCBT to PTB7-Th. Fullerene can be replaced by a nonfullerene acceptor without sacrifices in charge generation, achieving a PCE above 11%. These results support the idea that thermodynamic mixing and energetics of the polymer–polymer interface are critical design parameter for realizing highly efficient ternary solar cells with variable electron acceptors.


1. Introduction

Organic ternary bulk heterojunction (BHJ) blends containing two electron donating and one electron accepting organic moieties (or vice versa) are among the most auspicious material systems deemed promising to overcome the important barrier of 15% power conversion efficiency (PCE) of organic photovoltaic (OPV).^[1–8] Using a third semiconducting absorber in the bulk heterojunction blend, the three key photovoltaic parameters, short-circuit current density (J_{sc}),^[9–11] open-circuit voltage (V_{oc}),^[12,13] and fill factor (FF)^[14] can, in principle, be manipulated and enhanced compared to devices based on binary blends. The incorporation of a near-infrared (NIR) absorbing agent in particular may lead to a better match of the solar spectrum,^[15,16] resulting in enhanced J_{sc} , in analogy to conventional tandem and multijunction architectures, yet, maintaining the simplicity of fabrication of a single junction device. Moreover, adding polymers (or small molecules) with a higher lying lowest unoccupied molecular

Dr. N. Gasparini, Dr. S. Kahmann, Dr. M. Salvador, Dr. J. Dario Perea, Dr. N. Li, Dr. S. Rechberger, Prof. C. J. Brabec, Dr. T. Ameri
Institute of Materials for Electronics and Energy Technology (I-MEET)
Friedrich-Alexander-University Erlangen-Nuremberg
Martensstraße 7, 91058 Erlangen, Germany
E-mail: nicola.gasparini@kaust.edu.sa; christoph.brabec@fau.de; tayebbeh.ameri@lmu.de

Dr. S. Kahmann, Dr. G. Portale, Prof. M. A. Loi
Zernike Institute for Advanced Materials (ZIAM)
University of Groningen
Nijenborgh 4, 9747 AG, The Netherlands

Dr. A. Sperlich, Prof. V. Dyakonov
Experimental Physics VI
Julius-Maximilian University of Würzburg
97074 Würzburg, Germany

 The ORCID identification number(s) for the author(s) of this article can be found under <https://doi.org/10.1002/aenm.201803394>.

Dr. A. Baumann
Bavarian Center for Applied Energy Research (ZAE Bayern)
Magdalene-Schoch-Str. 3, 97074 Würzburg, Germany

Dr. S. Rechberger, E. Spiecker
Center for Nanoanalysis and Electron Microscopy (CENEM)
Friedrich-Alexander-University Erlangen-Nuremberg
Cauerstraße 6, 91058 Erlangen, Germany

Prof. C. J. Brabec
Bavarian Center for Applied Energy Research (ZAE Bayern)
Immerwahrstraße 2, 91058 Erlangen, Germany

Dr. T. Ameri
Chair of Physical Chemistry – Physical Chemistry and Nanoscience
Department of Chemistry
University of Munich (LMU)
Butenandtstrasse 5-13 (E), 81377 Munich, Germany

DOI: 10.1002/aenm.201803394

orbital level (closer to the vacuum level, E_{vac}), can lead to an increased V_{oc} .^[17] Finally, proper selection of the third component may facilitate exciton dissociation upon excitation,^[18] increase the charge carrier transport properties,^[14,19] and even lead to a more ideal morphology, affording ternary devices with improved FF.^[5,14] Despite these benefits, controlling the photovoltaic parameters independently or even collaboratively requires a fundamental understanding of the working mechanism of ternary bulk heterojunction blends. Such a degree of understanding has yet to be achieved as only few examples of high efficiency ternary blends clearly surpassing the binary counterparts have been reported so far.^[20–22]

In fact, the simultaneous enhancement of the photovoltaic parameters in ternary OPV blends continues to be challenging due to, in general terms, the difficulty of establishing a framework that identifies the chemical and physical parameters determining the efficiency enhancing compatibility of ternary blends.^[20] While the research community made important steps toward a global understanding of fundamental processes governing ternary devices, identifying, for instance, charge and energy transfer,^[23,24] parallel-like^[25] and alloy models,^[26,27] and combinations of those as relevant working mechanisms,^[9] we remain far from establishing general design rules for the fabrication of high performance ternary devices. Specifically, the mechanism by which additional photon energy that is gathered by the third component needs to be relayed in order to prevent thermalization losses and thus efficiently contribute to an enhancement in short-circuit current—without disrupting V_{oc} and FF—is poorly understood.^[28–30] We have recently demonstrated that the third component can act as charge relay material to overcome trap-assisted recombination

in amorphous binary blends, resulting in fill factors as high as 77%.^[14] Additionally, the ternary agent can operate as an antenna-like structure when the emission of the host material and absorption of the ternary agent overlap,^[31] favoring nonradiative Förster resonance energy transfer (FRET).^[18,32,33] The latter has been identified as an effective way to improve the PCE of BHJ solar cells. It is not uncommon, however, that both charge and energy transfer occur simultaneously, depending on the energetic alignment of the guest material.^[13] This raises the question about which mechanism may be most effective in transferring the extra photon energy with minimal losses in a ternary OPV blend. For this purpose, we study ternary organic solar cells based on a polymer–polymer system characterized by a very efficient FRET. As host material we used the polymer poly[5,5-bis(2-butylthiophenyl)-(2,2-bithiophene)-4,4-dicarboxylate-alt-5,5-2,2-bithiophene] (PDCBT, (Figure 1)),^[34] This is a thiophene-based polymer with a rather simple molecular structure that could potentially be produced at very low cost. When blended with the fullerene $PC_{70}BM$, a PCE of $\approx 7\%$ can be achieved. However, as discussed along the manuscript, this blend is limited by trap-assisted recombination. In order to overcome this limitation, we introduced the narrow bandgap polymer, PTB7-Th,^[35] resulting in an extended absorption window and delivering a PCE $> 10\%$, with a signature FF of 74%. The relatively high FF is a result of reduced charge carrier recombination. Moreover, we show that the polymers form a particular blend microstructure due to a higher intermolecular affinity (based on the Flory–Huggins theory) between PDCBT and PTB7-Th when compared with the affinity of either with the fullerene-derivative, which notably improves charge transport mechanism.

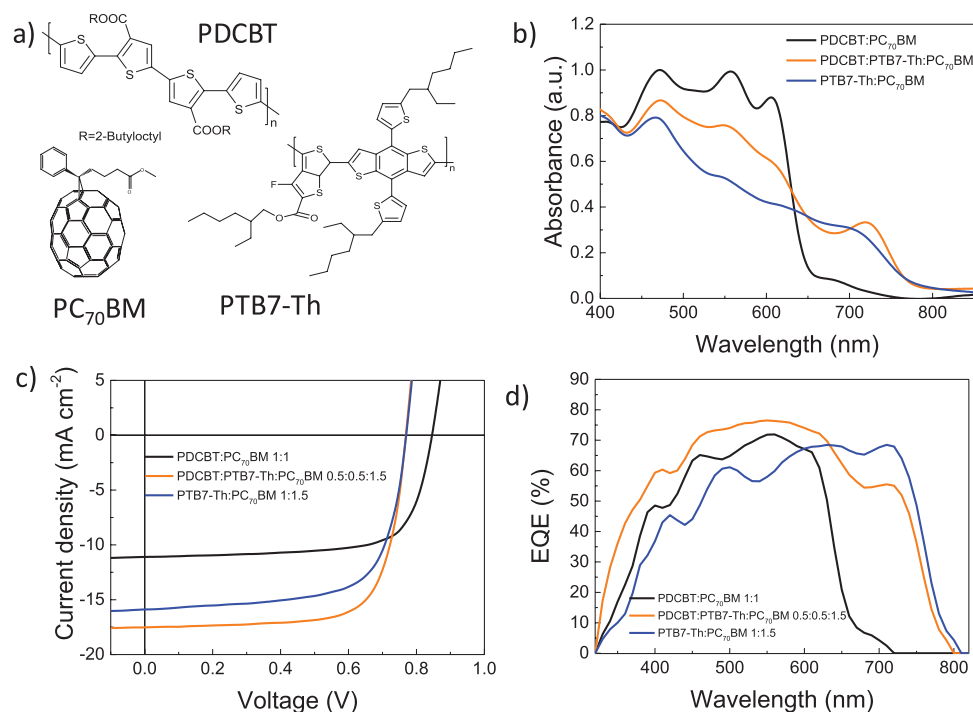


Figure 1. a) Molecular structure of the materials used. b) Absorption profiles of binary and ternary layers. c) Current–voltage characteristics of PDCBT:PC₇₀BM, PDCBT:PTB7-Th:PC₇₀BM, and PTB7-Th:PC₇₀BM based devices under 100 mW cm⁻² solar irradiance. d) External quantum efficiency curves of the same devices depicted in (c).

Table 1. Photovoltaic and charge transport properties of PDCBT:PC₇₀BM, PDCBT:PTB7-Th:PC₇₀BM, and PTB7-Th:PC₇₀BM solar cells. The average values for the power conversion efficiency were calculated over 20 devices.

PDCBT:PTB7-Th:PC ₇₀ BM	V _{oc} [V]	J _{sc} [mA cm ⁻²]	FF [%]	PCE [%]	μ [cm ² V ⁻¹ s ⁻¹]	n _t [cm ⁻³]	G [cm ⁻³ s ⁻¹]
1:0:1	0.85	11.11	66	6.23 (5.82 ± 0.25)	1.3 × 10 ⁻⁴	1.1 × 10 ¹⁶	7.68 × 10 ²¹
0.5:0.5:1.5	0.78	17.53	74	10.12 (9.84 ± 0.25)	4.1 × 10 ⁻⁴	9.12 × 10 ¹⁵	1.11 × 10 ²²
0:1:1.5	0.78	15.88	69	8.54 (8.23 ± 0.20)	2.8 × 10 ⁻⁴	9.18 × 10 ¹⁵	1.01 × 10 ²²

2. Result and Discussion

We fabricated organic BHJ ternary solar cells using an inverted device layout based on indium tin oxide (ITO)/ZnO/active layer/MoOx/Ag. In order to achieve the highest possible performance, we varied the amount of the NIR donor polymer (PTB7-Th), while the overall polymer to fullerene ratio was kept constant at 1:1.5 by weight. The chemical structures and the corresponding absorption spectra of the binary and ternary blends are depicted in Figure 1a,b, respectively. Table 1 summarizes the photovoltaic parameters for the BHJ solar cells. We achieved power conversion efficiencies of 6.2% and 8.5% for PDCBT:PC₇₀BM and PTB7-Th:PC₇₀BM reference blends, respectively. These efficiencies are in line with the current state-of-the-art for these types of solar cells.^[34,35]

Figure 1c shows the typical current density versus voltage (*J*-*V*) characteristics of the binary devices and the best ternary system under simulated AM 1.5G solar irradiation (100 mW cm⁻²). With the incorporation of 50% of PTB7-Th into the host PDCBT:PC₇₀BM, the V_{oc} approaches the V_{oc} of the binary blend PTB7-Th:PC₇₀BM. However, upon the addition of PTB7-Th we observed a significant increase in PCE, now exceeding 10%, mainly due to a considerable enhancement in J_{sc} of 37% and 9% compared to PDCBT:PC₇₀BM and PTB7-Th:PC₇₀BM binary devices, respectively, and a high FF of 74%. In order to confirm the current density values extracted from *J*-*V* measurements and to observe individual polymer contributions in the photon-to-current conversion efficiency, we performed external quantum efficiency (EQE) measurements. Figure 1d shows the extended spectral response of ternary devices compared to the host PDCBT-based binary device. The ternary devices feature a maximum EQE of 75% at ≈550 nm.

To elucidate the recombination landscape upon the addition of PTB7-Th into the host matrix of PDCBT:PC₇₀BM, we carried out additional current-voltage measurements under different light levels. First, we considered the recombination dynamics by probing the current-voltage behavior as a function of the light intensity for binary and ternary solar cells.^[36] In the V_{oc} versus light intensity plot in Figure 2a, the binary PDCBT:PC₇₀BM solar cells feature a slope of 1.21 kT q⁻¹, indicative of trap-assisted recombination, whereas we find slopes of 1.00 kT q⁻¹, i.e., pure second order recombination for both the ternary and the binary PTB7-Th:PC₇₀BM devices. Adding PTB7-Th into the binary PDCBT-matrix thus suppresses trap-induced charge carrier recombination. Previously, we have made similar observations in the case of other high efficiency ternary blends.^[14]

As a means to further analyze the presence of trap states in the PDCBT:PC₇₀BM blend, we performed thermally stimulated current (TSC) measurements.^[37] In TSC, trapped charge

carriers, which are initially generated by a light pulse or injected by an electrical field at very low temperatures (here 25 K), are probed by sensitively measuring the current while heating up the device to 300 K. Figure S1 (Supporting Information) depicts the TSC traces of both binary systems and of a ternary device with clearly detectable spectra between 25 and 200 K. By integrating the TSC spectrum over time, it is possible to calculate the lower limit trap density (n_t) (see the Experimental Section for details). In agreement with the trend observed in the V_{oc} versus light intensity measurements, we obtain n_t values of 1.1 × 10¹⁶, 9.1 × 10¹⁵, and 9.2 × 10¹⁵ cm⁻³ for PDCBT:PC₇₀BM, PDCBT:PTB7-Th:PC₇₀BM, and PTB7-Th:PC₇₀BM BHJ solar cells, respectively, confirming that PTB7-Th effectively decreases the trap density in PDCBT:PC₇₀BM binary blends. We note that recent simulations have shown that the presence of inhomogeneous carrier generation and distribution may lead to recombination exponents larger than 1 for systems that are mostly trap free.^[38] Although our interpretation matches accepted models of trap limited device performance in organic solar cells, we cannot exclude that inhomogeneous carrier generation and distribution may play a role in the systems presented here.

In addition, to examine the impact of light exposure on charge generation and charge transport, we measured the photocurrent density (J_{ph}) as a function of the effective voltage (V_{eff}).^[39,40] The J_{ph} versus V_{eff} traces in Figure 2b indicate that J_{ph} quickly saturates for V_{eff} below ≈1 V. Under this condition, all photogenerated electron-hole pairs are likely to dissociate and to be collected at the electrodes. This allows to estimate the maximum generation rate of free charge carriers G_{max} according to J_{sat} = qG_{max}L, where q is the electronic charge and L is the active layer thickness. The J_{sat} values for PDCBT:PC₇₀BM, PDCBT:PTB7-Th:PC₇₀BM, and PTB7-Th:PC₇₀BM BHJ solar cells extracted from Figure 2b are 12.30, 17.87, and 16.19 mA cm⁻², leading to G_{max} values of 7.68 × 10²¹, 1.12 × 10²², and 1.01 × 10²² cm⁻³ s⁻¹, respectively. The increase in G_{max} in the ternary blend is consistent with the improved J_{sc} values extracted under solar simulator illumination. This finding underscores the ability of PTB7-Th to enhance the photocurrent in ternary blends. Table 1 summarizes all relevant photophysical parameters for the binary and ternary systems.

We now turn the attention to the working mechanism of the ternary blend PDCBT:PTB7-Th:PC₇₀BM in devices. We first analyzed the charge transport behavior by investigating the charge carrier mobility μ of devices comprising the three different blend systems using photoinduced charge carrier extraction by linearly increasing voltage (photo-CELIV).^[41] Figure 2c shows the corresponding photo-CELIV transients. The traces were recorded by applying a 2 V/60 μs linearly increasing reverse bias pulse and a delay time (t_d) of 1 μs. From the

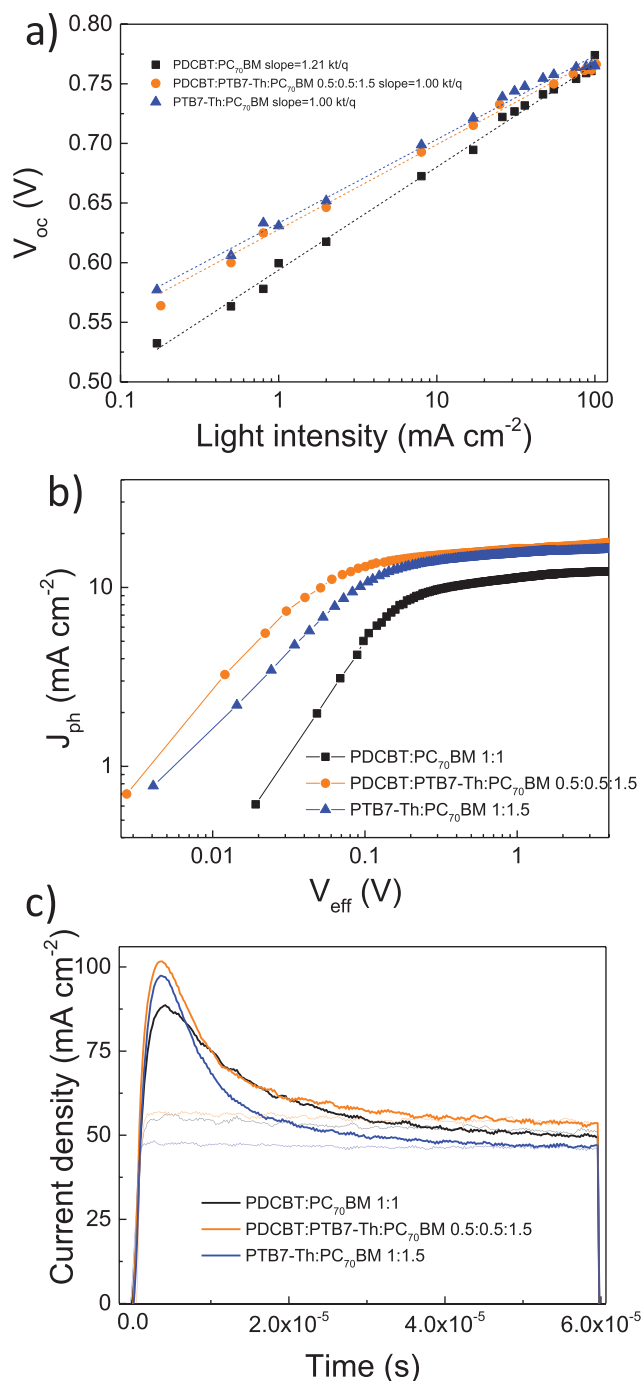


Figure 2. a) Open-circuit voltage as a function of light intensity of PDCBT:PC₇₀BM, PDCBT:PTB7-Th:PC₇₀BM, and PTB7-Th:PC₇₀BM BHJ solar cells and b) photocurrent in reverse polarization for the same solar cells. The photocurrent J_{ph} is defined as $J_{ph} = J_l - J_d$, where J_l and J_d are the current density under illumination and in the dark, respectively, while the effective voltage V_{eff} is given by $V_{eff} = V_0 - V$, where V_0 is the compensation voltage defined as $J_{ph}(V_0) = 0$, and V is the applied voltage. c) Photo-CELIV traces for PDCBT:PC₇₀BM, PDCBT:PTB7-Th:PC₇₀BM, and PTB7-Th:PC₇₀BM BHJ solar cells.

measured photocurrent we calculated mobilities of 1.3×10^{-4} , 4.1×10^{-4} , and $2.8 \times 10^{-4} \text{ cm}^2 \text{ V}^{-1} \text{ s}^{-1}$ for the PDCBT:PC₇₀BM, PDCBT:PTB7-Th:PC₇₀BM, and PTB7-Th:PC₇₀BM BHJ solar

cells, respectively (see the Experimental Section for details). It is plausible that the higher mobility values calculated for the ternary blend contribute to an increase in FF as reported in Table 1, confirming that the introduction of the PTB7-Th improves the charge transport properties compared to both binary devices.

The photovoltaic performance and the charge transport/recombination characteristics presented above suggest that the incorporation of the second polymer simultaneously leads to a lower amount of trap states, an increase in charge carrier generation and higher charge carrier mobilities than found in both reference binary devices. To clarify the origin of this improvement, we investigated the interaction of the three components upon photoexcitation using steady-state and transient spectroscopic techniques as will be discussed below. First, we considered the results of steady-state and ultrafast time-resolved photoluminescence spectroscopy of films of the neat materials, the binary blends, and the ternary blend upon excitation at 400 nm. Interestingly, as depicted in Figure 3a, the photoluminescence (PL) of the PDCBT:PTB7-Th binary blend resembles the spectrum of PTB7-Th, while the emission of PDCBT is fully quenched. Considering the transient PL measurements shown in Figure S2 of the Supporting Information (taken around maximum emission intensity) and the fitted lifetimes in Table S1 of the Supporting Information, this quenching behavior can be attributed to either energy transfer from the wider bandgap polymer PDCBT to PTB7-Th or a strikingly asymmetric charge transfer step, i.e., rapid electron transfer from PDCBT to PTB7-Th, whereas the opposite process is energetically hampered.

Notably, there is a broad overlap between the emission of PDCBT and the absorption of PTB7-Th (Figure S3, Supporting Information), possibly allowing for a Förster-like energy-transfer process between these two polymers. We thus examined the photoluminescence of PDCBT:PTB7-Th films as a function of the concentration (1% to 20%) of the supposed acceptor (PTB7-Th). From the steady state spectra in Figure S4a of the Supporting Information it is apparent that at a very low acceptor concentration of 1% the emission of PDCBT is already significantly reduced. At concentrations of PTB7-Th above 5% the quenching of the PDCBT emission is close to complete (exceeding 98%, see Table S1, Supporting Information). Concomitantly, the PDCBT photoluminescence lifetime (where extractable) continuously decreases upon adding PTB7-Th (Figures S4b, Supporting Information).

The time resolved emission of PTB7-Th, by contrast, strikingly exhibits not only an increased PL lifetime, but more importantly, a delayed maximum of PL intensity for low PTB7-Th concentrations (Figure 3b). Such a behavior is evidence for energy transfer from PDCBT toward PTB7-Th.^[42,43] Generally, an effect of this magnitude is consistent with both fine intermixing of the two components and a long PL lifetime of neat PDCBT, allowing excitons in this material to travel long distances before encountering PTB7-Th regions.

With clear evidence for energy transfer at hand, we turned to steady-state photoinduced absorption (PIA) spectroscopy to probe the nature of the charge carriers present in polymer-fullerene and ternary blends. We first studied the mid-infrared (MIR) spectral region using a modified FTIR spectrometer.^[44] We performed measurements at energies as low as 0.08 eV, i.e.,

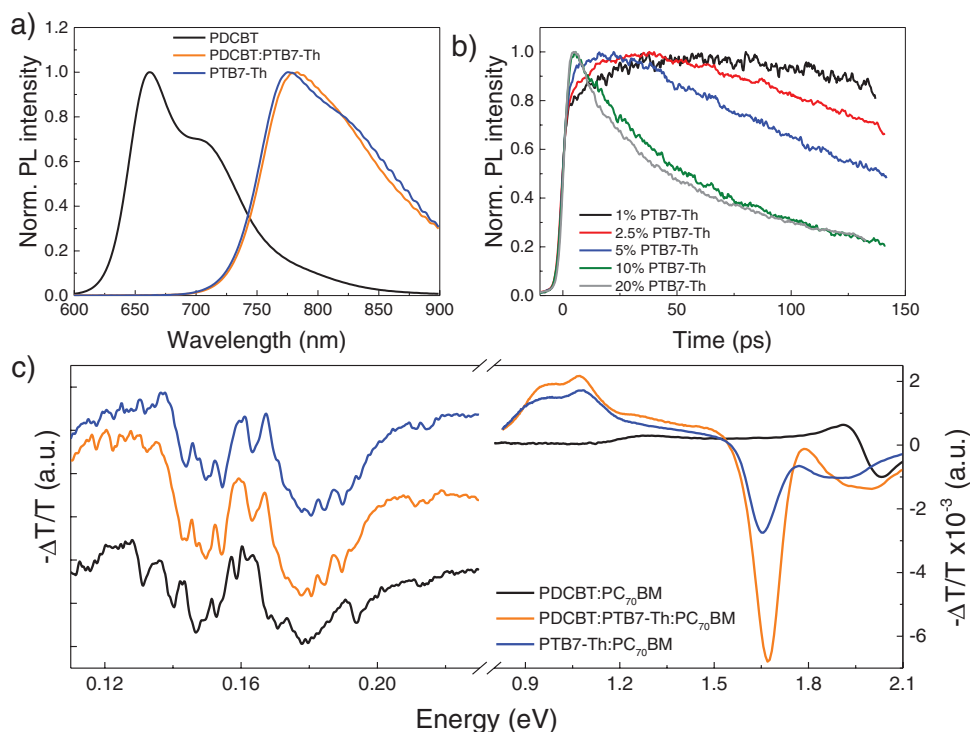


Figure 3. a) Steady-state photoluminescence of PDCBT, PDCBT:PTB7-Th (1:1) and PTB7-Th excited at 400 nm. b) Time resolved PL of PDCBT:PTB7-Th blends with different PTB7-Th concentration, monitored for the emission of PTB7-Th at 800 nm. c) Photo-induced absorption spectroscopy in the MIR–NIR–vis region for binary and ternary blends.

the region characteristic of low energy polaron transitions as well as signatures due to molecular vibrations of the polymer backbone (infrared active vibrations; IRAVs) that may be used as material specific fingerprints.^[45,46] PTB7-Th:PC₇₀BM, exhibits a broad absorption feature between ≈ 0.1 – 0.4 eV, which is superimposed with IRAVs and two broader dips around 0.2 eV (Figure S5a, green, Supporting Information), which we attribute to the P1 transition of the polymer polaron. The PDCBT:PC₇₀BM blend leads to a similar signature (Figure S5b, Supporting Information) consisting of a broad signal between 0.2 and 0.3 eV, again superimposed with vibrational features. Comparing the two binary blends with each other (Figure 3c), we find indicators that allow to distinguish the two polymers—notably the less pronounced band for PDCBT around 0.22 eV, the slope at 0.13 eV and, most prominently, the band at 0.14 eV, which comprises three narrow features for PDCBT and two (further apart) for PTB7-Th. In the case of the ternary blend, we only find evidence for the PTB7-Th polaron (Figure 3c). We thus assume that PDCBT does not significantly contribute to charge generation in the ternary blend and the electron transfer toward PC₇₀BM to be outcompeted by the energy transfer to PTB7-Th.

To support our interpretation with a more commonly employed technique, we studied the PIA spectra in the visible and near-infrared spectral region that allows for probing ground state bleaching and higher polaron transitions, respectively.^[21,47,48] Figure 3c depicts the in-phase PIA signals of the different blends between ≈ 0.8 and 2.1 eV. The two polymer–fullerene blends exhibit a distinct photobleach (PB) around 2.07 eV for PDCBT and 1.68 eV for PTB7-Th. Interestingly,

PTB7-Th:PC₇₀BM and PDCBT:PTB7-Th:PC₇₀BM both feature a strong photoinduced absorption signal between ≈ 0.8 and 1.1 eV. PDCBT:PC₇₀BM, by contrast, shows no signal below 1.1 eV. The PDCBT polaron is located at ≈ 1.25 eV, similar to P3HT, i.e., the polarons of PDCBT and PTB7-Th are spectrally separated. In the case a ternary blend film, the amplitude of the polaron signal for PTB7-Th (at 0.8–1.2 eV) is larger by a factor of >2 when compared with the polaron signal for PDCBT. The combination of these observations supports our claim that holes relevant for charge transport in a ternary solar cell reside predominantly on PTB7-Th and are likely efficiently transported through PTB7-Th interconnects.

We further confirmed this picture by measuring the polaron fingerprints in binary and ternary composites using X-band electron paramagnetic resonance (EPR) spectroscopy (Figure 4).^[49] For these measurements, blends with PC₆₀BM instead of PC₇₀BM were used, because the resulting polaronic EPR signatures of the polymer and fullerene do not overlap and are therefore easier to interpret.^[50] The morphology is not influenced by the choice of the PCBM derivative. The traces unambiguously confirm that the positive polarons in the case of the ternary blend PDCBT:PTB7-Th:PCBM are mainly located in the PTB7-Th matrix. This conclusion is possible because the signals for the PTB7-Th:PCBM and PDCBT:PTB7-Th:PCBM overlay, while the trace for PDCBT:PCBM is clearly shifted toward lower *g*-factors/higher magnetic fields.

As predicted by the Förster resonance energy theory, the FRET efficiency scales inversely with the 6th power of the distance between donor and acceptor.^[18] Therefore, a ternary blend morphology in which both species—in our case PDCBT

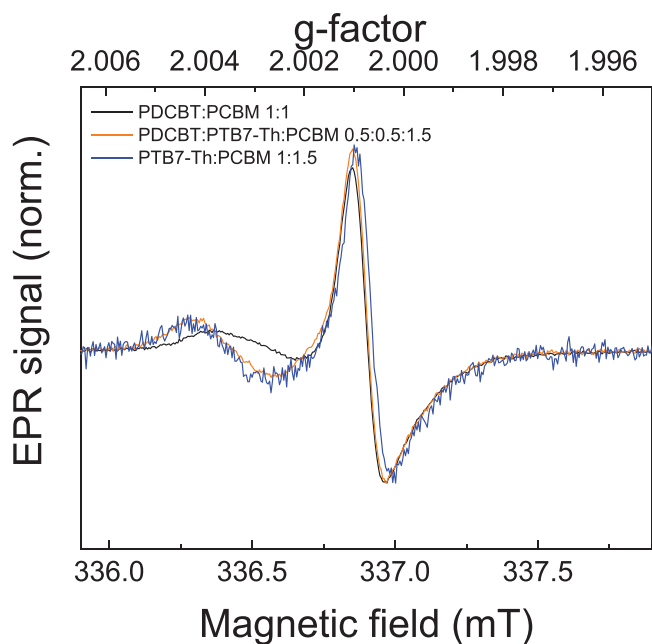


Figure 4. X-band EPR spectra of the blends PTB7-Th:PCBM, PDCBT:PTB7-Th:PCBM, and PDCBT:PCBM at 70 K using white light LED illumination. Signals were normalized at the lower right peak of PC₆₀BM⁻ to facilitate comparison of the polymer⁺ signal.

and PTB7-Th—are in close proximity is a stringent requirement for its presence. To understand how the morphology plays into the optoelectronic properties of ternary devices based on PDCBT:PTB7-Th:PC₇₀BM, we first investigated blend films using energy-filtered transmission electron microscopy (EFTEM).

Figure 5a–c shows EFTEM images at an energy loss of 267 ± 15 eV of PDCBT:PC₇₀BM, PDCBT:PTB7-Th:PC₇₀BM, and PTB7-Th:PC₇₀BM films, while Figure S6 of the Supporting Information displays elemental maps based on EFTEM images of carbon (C) using the C K edge and of sulfur (S) using the S L edge.^[51] The carbon and sulfur signals can both be used to identify PC₇₀BM (C-PC₇₀BM = 83,7 at%, C-PTB7-Th = 44,2 at%, and C-PDCBT = 38,9 at%) and polymer rich phases (S-PTB7-Th = 4.4 at% and S-PDCBT = 3.7 at%) with good contrast. In the case of PDCBT:PC₇₀BM (Figure 5a), we observe the formation of fiber-like structures. This morphological motif is common among thiophene-based materials. By contrast, PTB7-Th:PC₇₀BM shows a microstructure that reflects the

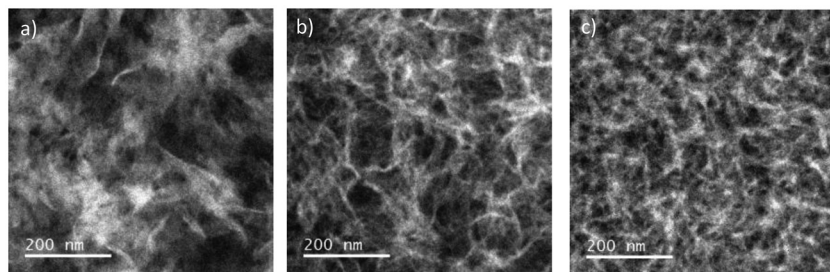


Figure 5. EFTEM images at an energy loss of 267 ± 15 eV of a) PDCBT:PC₇₀BM, b) PDCBT:PTB7-Th:PC₇₀BM, and c) PTB7-Th:PC₇₀BM films. Dark areas correspond to PC₇₀BM rich domains.

well-known amorphous nature of the polymer.^[35] Interestingly, the PDCBT:PTB7-Th:PC₇₀BM blend features an even more pronounced fibrillar structure.^[52] Based on the EFTEM investigation we suggest that amorphous PTB7-Th accumulates around prearranged PDCBT fibers in the ternary blend. Given that FRET is more likely to occur for close distances between the donor and the acceptor, we hypothesize that this particular configuration promotes an efficient FRET from PDCBT to PTB7-Th. After this initial energy transfer step, electron transfer from PTB7-Th to surrounding PC₇₀BM is likely to occur (Figure S7, Supporting Information).

The molecular packing in the pure components, in the binary and the ternary blends was studied by using grazing incidence wide-angle X-ray scattering (GIWAXS) (Figures S8 and S9, Supporting Information). The pure PDCBT polymer shows high crystallinity with lamellar-like structure and molecular orientation in an edge-on configuration, exhibiting a strong first-order Bragg reflection centered at about 3 nm^{-1} (characteristic spacing of 2.1 nm) followed by 3 to 4 clear high order reflections, in agreement with previous reports.^[34] The PDCBT:PC₇₀BM binary blend exhibits lower crystallinity with respect to pure PDCBT with only one main diffraction arc centered at 3.1 nm^{-1} . In the binary blend with PC₇₀BM, the PDCBT molecules still adopt predominantly an edge-on orientation with respect to the substrate. In addition, the PDCBT:PC₇₀BM blend features a ring located at $q \approx 14 \text{ nm}^{-1}$ that can be linked to PC₇₀BM domains. In contrast to PDCBT, both pure PTB7-Th and its binary blend with PC₇₀BM show lower degree of order and minor preferential orientation of the molecules with respect to the substrate. The diffraction ring for the pure PTB7-Th polymer is located at $q \approx 2.7 \text{ nm}^{-1}$ (spacing of 2.3 nm). The binary blend of the two PDCBT and PTB7-th polymers shows only one main signal located at $q \approx 2.8 \text{ nm}^{-1}$, suggesting some degree of mixing between the two polymers and reduced crystallinity with respect to pure PDCBT. In analogy to the binary blend, the ternary PDCBT:PTB7-Th:PC₇₀BM blend also shows a reduced order and exhibits a single peak at $q \approx 2.8 \text{ nm}^{-1}$ and a spacing of 2.2 nm. The molecules show a lower degree of alignment with respect to the substrate when compared to pure PDCBT and its binary blend with PCBM, although the predominant orientation remains edge-on. Overall, this suggests that the fibers are no longer highly crystalline PDCBT fibers but instead already somewhat blended with PTB7-Th at the polymer–polymer interface and the PDCBT host most probably acts as a template for aligning PTB7-Th. Furthermore, the ring at $q \approx 14 \text{ nm}^{-1}$ suggests the presence of PCBM domains. A summary of the GIWAXS results is reported in Table S2 of the Supporting Information.

The fact that PTB7-Th preferentially aligns along PDCBT features rather than mixing with PCBM is a key signature of this ternary blend. To elucidate this peculiar mixing behavior, we calculated the intermolecular parameters $X_{1,2}$ of the two polymers with respect to PC₇₀BM using a thermodynamic mixing model based on Flory–Huggins solution theory that we have reported elsewhere.^[53,54] Typically, a value of $X_{1,2}$ toward 0 is indicative of good miscibility while

higher values represent a reduced tendency for intermixing. Table S3 of the Supporting Information shows the values of $X_{1,2}$ for polymer:polymer and polymer:fullerene blends. Comparison of the intermolecular parameters reveal the lowest $X_{1,2}$ of 0.20 for PDCBT:PTB7-Th when compared to PDCBT:PC₇₀BM ($X_{1,2}$ of 2.29) and PTB7-Th:PC₇₀BM ($X_{1,2}$ of 1.23). This analysis indicates that PTB7-Th has a higher driving force to mix with PDCBT than mixing with the fullerene. This outcome is important for two reasons. It corroborates the morphological picture that PTB7-Th prefers to align with PDCBT rather than intermixing with PCBM. According to our photophysical analysis, this favors the occurrence of FRET without sacrificing exciton splitting at the polymer–fullerene interface. Furthermore, and more generally, this thermodynamic mixing model could be used for evaluating the compatibility and suitability of polymers and small molecules for photovoltaic ternary blends.

3. Conclusion

In conclusion, we designed ternary polymer–fullerene blend based on the polythiophene PDCBT, the prototypical copolymer PTB7-Th and PC₇₀BM. Optimized ternary blends incorporated into a very simple, inverted device layout using ZnO and MoOx as charge extraction layers consistently increase the power conversion efficiency of PDCBT:PC₇₀BM and PTB7-Th:PC₇₀BM blend devices by 39% and 15%, respectively, to beyond 10%. Notably, the ternary blend features an FF of 74%, significantly higher than either of the two binary blends. We conclude that this phenomenon is closely linked to the favorable morphology that is adopted by the three components. The fairly low intermolecular parameter between PDCBT and PTB7-Th allows the polymers to take on a common orientation and manifest strong polymer–polymer interactions. This dominates the photo-physics of this blend, which is mainly founded on an efficient energy transfer process (FRET) that quickly relays harvested energy from PDCBT to PTB7-Th. The addition of PTB7-Th further improves the charge transfer mechanism and recombination characteristics of PDCBT. The strong molecular affinity between the polymers anticipates that other electron accepting units will similarly arrange around the PDCBT:PTB7-Th fibers. In fact, when replacing fullerene with a nonfullerene acceptor using the same optimal ratio as in the case of PDCBT:PTB7-Th:PC₇₀BM, we readily achieve 11.2% power conversion efficiency using IEICO-4Cl^[55] as electron accepting unit (Figure S10 and Table S4, Supporting Information), whereas the binary devices delivered lower PCE of 6.3% and 9.4% for PDCBT:IEICO-4Cl and PTB7-Th:IEICO-4Cl, respectively. In analogy with the fullerene-based ternary devices, PDCBT:PTB7-Th:IEICO-4Cl shows reduced trap-assisted recombination (Figure S10d, Supporting Information) and higher charge carrier mobility (Figure S10e, Supporting Information) compared to the binary devices, justifying the molecular affinity between the two donor polymers regardless the small molecule acceptor used.

In the recent past, we have identified several examples, in which the addition of a semiconducting, mostly amorphous polymer with superior charge transport behavior is capable of passivating traps in the bulk of charge transport limited binary

blends. However, the interplay between trap passivation and a suitable morphology remains critical. For instance, we have observed reductions in power conversion efficiency for systems, which are limited by morphology,^[21] despite a very favorable reduction of the trap density. Thus, evaluation of the mixing thermodynamics based on Flory–Huggins theory contributes to the understanding of the intricate morphology of ternary blends. We suggest that the intermolecular parameter should be considered as a physical quantity to further improve the design of multinary, panchromatic organic solar cell blends.

4. Experimental Section

Materials: PCDBT ($M_w = 70$ kDa) and PTB7-Th ($M_w = 180$ kDa) were purchased from 1-Materials, PC₇₀BM was purchased from Solenne PV.

Device Fabrication and Measurements: Prestructured indium tin oxide (ITO) substrates were cleaned with acetone and isopropyl alcohol in an ultrasonic bath for 10 min each. After drying, the substrates were doctor bladed with 40 nm of zinc oxide (ZnO) and a ≈100 nm thick active layer based on binary and ternary blends (25 g L⁻¹ in a mixture of chlorobenzene (CB) and 1,8-diodooctane 97 to 3 vol%). To complete the fabrication of the devices 10 nm of MoOx and 100 nm of Ag were thermally evaporated through a mask (with a 10.4 mm² active area opening) under a vacuum of ≈1 × 10⁻⁶ mbar. The J - V characteristics were measured using a source measurement unit from a homemade setup. Illumination was provided by a solar simulator (Oriol Sol 1A, from Newport) with AM1.5G spectrum at 100 mW cm⁻². In order to study the light intensity dependence of current density, a series of neutral color density filters was used. The intensity of light transmitted through the filter was independently measured via a power meter. UV–vis absorption was performed on a Lambda 950, from Perkin Elmer. EQEs were measured using an integrated system from Enlitech, Taiwan. All the devices were tested in ambient air.

Photo-CELIV Measurements: The devices were illuminated using a 780 nm laser-diode. Current transients were recorded across an internal 50 Ω resistor of an oscilloscope (Agilent Technologies DSO-X 2024A). A fast electrical switch was used to isolate the cell and prevent charge extraction or sweep out during the laser pulse and the delay time. After a variable delay time, a linear extraction ramp was applied via a function generator. The ramp, which was 60 μs long and 2 V in amplitude, was set to start with an offset matching the V_{oc} of the cell for each delay time. From the measured photocurrent transients, the charge carrier mobility (μ) can be calculated using Equation (1)

$$\mu = \frac{2d^2}{3At^2_{\max} \left[1 + 0.36 \frac{\Delta j}{j(0)} \right]} \text{ if } \Delta j \leq j(0) \quad (1)$$

where d is the active layer thickness, A is the voltage rise speed $A = dU/dt$, U is the applied voltage, t_{\max} is the time corresponding to the maximum of the extraction peak, and $j(0)$ is the displacement current.

Photoluminescence: Films were deposited on quartz substrates, mounted into a nitrogen filled sample holder, and excited at 400 nm using the second harmonic of a mode-locked Ti:sapphire laser at a repetition rate of 76 MHz. Steady-state spectra were recorded with an InGaAs detector from Andor. Time resolved traces were taken with a Hamamatsu streak camera working in synchroscan mode.

PIA: For MIR investigations, solutions were spin cast on ZnSe substrates and mounted into a cryostat without having been exposed to air. To avoid perturbations from the pump light, a GaAs filter was placed in front of the detector. Spectra were acquired with a resolution of 5 cm⁻¹ and the measurement cycle was run at least 512 times.^[44] Quasi-steady-state PIA studies in the NIR were performed by exciting the sample with a 532 nm laser, chopped at 141 Hz, and probing with the

continuous spectrum of a Xe lamp. The transmitted light is dispersed by a 1200 lines mm⁻¹ grating monochromator (iHR320, Horiba) and detected by a Si detector down to an energy of 1.1 eV and an InGaAs detector for lower values. Additional measurements with a blocked Xe lamp account for the sample PL. In both cases, measurements occurred at cryogenic temperature.

TSC: TSC measurements were conducted in a closed-cycle He cryostat, with Helium as a contact gas for thermal coupling. To avoid any atmospheric exposure, solar cells were transferred via an integrated sample lock system from a glove box to the cryostat. In TSC, the samples is first cooled down to very low temperatures (here: 25 K) and then illuminated by an LED array for 10 min to create charge carriers, which thermalize to the deepest available states in the density of states. After a dwell time of 10 min in the darkness, the sample was heated up to 300 K at a constant rate of 7 K min⁻¹. The TSC signal of the sample was detected by a Sub-Femtoamp Remote Source Meter (Keithley 6430) without the application of a bias voltage. It is noted that the TSC signal describes only a lower limit. Traps might not be completely filled by the light pulse or some of the charge carriers may recombine with oppositely charged carriers during the release process. In both cases, the actual trap concentration may be larger than determined by the integration of the TSC peak.

EPR: Samples were prepared by doctor blading the active layer on plastic foil. This was cut into slices of which 10 were stacked into 3 mm EPR sample tubes that were subsequently sealed under inert helium atmosphere. A modified X-band spectrometer (Bruker E300) was used with illumination provided by a white light LED with ≈1 sun intensity at the sample position inside a continuous flow helium cryostat. The g-factor was calibrated for each measurement with the help of a NMR Gaussmeter (Bruker ER035M) and a microwave frequency counter.

TEM: The active layers for the TEM investigations were prepared as plan view specimens. Therefore, films of PEDOT:PSS and PIDTTQ:PC₇₀BM with a thickness of 50 nm were deposited on glass using doctor-blading under ambient conditions. To float off the active layer, the sample was put into a vessel with distilled water, where PEDOT:PSS dissolved, and the active layer was transferred to a Cu TEM supporting grid. The TEM investigations were performed using an FEI Titan Themis³ 300 TEM with a high brightness field emission gun (X-FEG) operated at 200 kV equipped with a high-resolution Gatan Imaging Filter (GIF Quantum) used for electron energy-loss spectroscopy and EFTEM. Elemental maps were calculated using the three-window-technique.

Supporting Information

Supporting Information is available from the Wiley Online Library or from the author.

Acknowledgements

The authors gratefully acknowledge the support of the Cluster of Excellence “Engineering of Advanced Materials” at the University of Erlangen-Nuremberg, which was funded by the German Research Foundation (DFG) within the framework of its “Excellence Initiative,” Synthetic Carbon Allotropes (SFB953) and Solar Technologies go Hybrid (SolTech). M.S. acknowledges primary support from a fellowship by the Portuguese Fundação para a Ciência e a Tecnologia (SFRH/BPD/71816/2010). S.K. sincerely thanks the Ubbo Emmius foundation of the University of Groningen and the research training group GRK 1896 the German Research foundation for funding of his Ph.D. T.A. acknowledges financial support of the German Research Foundation (DFG project with Grant No. AM 519/1-1). The work at the University of Würzburg was supported by the German Research Foundation (DFG) within the GRK2112.

Conflict of Interest

The authors declare no conflict of interest.

Keywords

FRET, high efficiency, mixing thermodynamics, photophysics, ternary organic solar cells

Received: November 3, 2018

Revised: March 8, 2019

Published online: April 1, 2019

- [1] N. Gasparini, A. Salleo, I. McCulloch, D. Baran, *Nat. Rev. Mater.* **2019**, 1, 1.
- [2] Q. An, F. Zhang, J. Zhang, W. Tang, Z. Deng, B. Hu, *Energy Environ. Sci.* **2016**, 9, 281.
- [3] T. Ameri, P. Khoram, J. Min, C. J. Brabec, *Adv. Mater.* **2013**, 25, 4245.
- [4] T. Kumari, S. M. Lee, S. Kang, S. Chen, C. Yang, *Energy Environ. Sci.* **2017**, 10, 258.
- [5] J. Zhang, Y. Zhang, J. Fang, K. Lu, Z. Wang, W. Ma, Z. Wei, *J. Am. Chem. Soc.* **2015**, 137, 8176.
- [6] D. Baran, R. S. Ashraf, D. A. Hanifi, M. Abdelsamie, N. Gasparini, J. A. Röhr, S. Holliday, A. Wadsworth, S. Lockett, M. Neophytou, C. J. M. Emmott, J. Nelson, C. J. Brabec, A. Amassian, A. Salleo, T. Kirchartz, J. R. Durrant, I. McCulloch, *Nat. Mater.* **2017**, 16, 363.
- [7] M. Nam, M. Cha, H. H. Lee, K. Hur, K.-T. Lee, J. Yoo, I. K. Han, S. J. Kwon, D.-H. Ko, *Nat. Commun.* **2017**, 8, 14068.
- [8] H. Li, K. Lu, Z. Wei, *Adv. Energy Mater.* **2017**, 7, 1602540.
- [9] N. Gasparini, L. Lucera, M. Salvador, M. Prosa, G. D. Spyropoulos, P. Kubis, H.-J. Egelhaaf, C. J. Brabec, T. Ameri, *Energy Environ. Sci.* **2017**, 10, 885.
- [10] F. Zhao, Y. Li, Z. Wang, Y. Yang, Z. Wang, G. He, J. Zhang, L. Jiang, T. Wang, Z. Wei, W. Ma, B. Li, A. Xia, Y. Li, C. Wang, *Adv. Energy Mater.* **2017**, 7, 1602552.
- [11] L. Lu, T. Xu, W. Chen, E. S. Landry, L. Yu, *Nat. Photonics* **2014**, 8, 716.
- [12] P. Cheng, Y. Li, X. Zhan, *Energy Environ. Sci.* **2014**, 7, 2005.
- [13] L. Lu, W. Chen, T. Xu, L. Yu, *Nat. Commun.* **2015**, 6, 7327.
- [14] N. Gasparini, X. Jiao, T. Heumueller, D. Baran, G. J. Matt, S. Fladischer, E. Spiecker, H. Ade, C. J. Brabec, T. Ameri, *Nat. Energy* **2016**, 1, 16118.
- [15] H. Cha, D. S. Chung, S. Y. Bae, M. J. Lee, T. K. An, J. Hwang, K. H. Kim, Y. H. Kim, D. H. Choi, C. E. Park, *Adv. Funct. Mater.* **2013**, 23, 1556.
- [16] J. Zhang, G. Xu, F. Tao, G. Zeng, M. Zhang, Y. (Michael) Yang, Y. Li, Y. Li, *Adv. Mater.* **2019**, 31, 1807159.
- [17] P. P. Khlyabich, B. Burkhart, B. C. Thompson, *J. Am. Chem. Soc.* **2011**, 133, 14534.
- [18] V. Gupta, V. Bharti, M. Kumar, S. Chand, A. J. Heeger, *Adv. Mater.* **2015**, 27, 4398.
- [19] S. Liu, P. You, J. Li, J. Li, C.-S. Lee, B. S. Ong, C. Surya, F. Yan, *Energy Environ. Sci.* **2015**, 8, 1463.
- [20] Y. (Michael) Yang, W. Chen, L. Dou, W. Chang, H. Duan, B. Bob, G. Li, Y. Yang, *Nat. Photonics* **2015**, 9, 190.
- [21] N. Gasparini, M. Salvador, S. Fladischer, A. Katsouras, A. Avgeropoulos, E. Spiecker, C. L. Chochos, C. J. Brabec, T. Ameri, *Adv. Energy Mater.* **2015**, 5, 1501527.
- [22] X. Song, N. Gasparini, M. M. Nahid, S. H. K. Paleti, J. Wang, H. Ade, D. Baran, *Joule* **2019**, 3, 846.
- [23] H. Löslein, T. Ameri, G. J. Matt, M. Koppe, H. J. Egelhaaf, A. Troeger, V. Sgobba, D. M. Guldi, C. J. Brabec, *Macromol. Rapid Commun.* **2013**, 34, 1090.

- [24] S. Honda, H. Ohkita, H. Benten, S. Ito, *Chem. Commun.* **2010**, 46, 6596.
- [25] L. Yang, H. Zhou, S. C. Price, W. You, *J. Am. Chem. Soc.* **2011**, 134, 5432.
- [26] R. A. Street, D. Davies, P. P. Khlyabich, B. Burkhart, B. C. Thompson, *J. Am. Chem. Soc.* **2013**, 135, 986.
- [27] P. Cheng, C. Yan, Y. Wu, J. Wang, M. Qin, Q. An, J. Cao, L. Huo, F. Zhang, L. Ding, Y. Sun, W. Ma, X. Zhan, *Adv. Mater.* **2016**, 28, 8021.
- [28] C. Wang, W. Zhang, X. Meng, J. Bergqvist, X. Liu, Z. Genene, X. Xu, A. Yartsev, O. Inganäs, W. Ma, E. Wang, M. Fahlman, *Adv. Energy Mater.* **2017**, 7, 1700390.
- [29] N. Felekidis, E. Wang, M. Kemerink, *Energy Environ. Sci.* **2016**, 9, 257.
- [30] B. M. Savoie, S. Dunaisky, T. J. Marks, M. A. Ratner, *Adv. Energy Mater.* **2015**, 5, 1400891.
- [31] L. Ke, J. Min, M. Adam, N. Gasparini, Y. Hou, J. D. Perea, W. Chen, H. Zhang, S. Fladischer, A.-C. Sale, E. Spiecker, R. R. Tykwinski, C. J. Brabec, T. Ameri, *Adv. Energy Mater.* **2016**, 6, 1502355.
- [32] W.-L. Xu, B. Wu, F. Zheng, X.-Y. Yang, H.-D. Jin, F. Zhu, X.-T. Hao, *J. Phys. Chem. C* **2015**, 119, 21913.
- [33] L. Zhang, X. Xu, B. Lin, H. Zhao, T. Li, J. Xin, Z. Bi, G. Qiu, S. Guo, K. Zhou, X. Zhan, W. Ma, *Adv. Mater.* **2018**, 30, 1805041.
- [34] M. Zhang, X. Guo, W. Ma, H. Ade, J. Hou, *Adv. Mater.* **2014**, 26, 5880.
- [35] Z. He, B. Xiao, F. Liu, H. Wu, Y. Yang, S. Xiao, C. Wang, T. P. Russell, Y. Cao, *Nat. Photonics* **2015**, 9, 174.
- [36] L. J. A. Koster, V. D. Mihailetschi, R. Ramaker, P. W. M. Blom, *Appl. Phys. Lett.* **2005**, 86, 123509.
- [37] J. Schafferhans, A. Baumann, A. Wagenpfahl, C. Deibel, V. Dyakonov, *Org. Electron.* **2010**, 11, 1693.
- [38] A. V. Nenashev, M. Wiemer, A. V. Dvurechenskii, L. V. Kulik, A. B. Pevtsov, F. Gebhard, M. Koch, S. D. Baranovskii, *Phys. Rev. B* **2017**, 104207, 1.
- [39] S. R. Cowan, A. Roy, A. J. Heeger, *Phys. Rev. B* **2010**, 82, 245207.
- [40] N. Gasparini, M. Salvador, T. Heumueller, M. Richter, A. Classen, S. Shrestha, G. J. Matt, S. Holliday, S. Strohm, H.-J. Egelhaaf, A. Wadsworth, D. Baran, I. McCulloch, C. J. Brabec, *Adv. Energy Mater.* **2017**, 7, 1701561.
- [41] T. M. Clarke, C. Lungenschmied, J. Peet, N. Drolet, A. J. Mozer, *Adv. Energy Mater.* **2015**, 5, 1401345.
- [42] G. Bongiovanni, C. Botta, G. Di Silvestro, M. A. Loi, A. Mura, R. Tubino, *Chem. Phys. Lett.* **2001**, 345, 386.
- [43] H. Neugebauer, M. A. Loi, C. Winder, N. S. Sariciftci, G. Cerullo, A. Gouloumis, P. Vázquez, T. Torres, *Sol. Energy Mater. Sol. Cells* **2004**, 83, 201.
- [44] S. Kahmann, D. Fazzi, G. J. Matt, W. Thiel, M. A. Loi, C. J. Brabec, *J. Phys. Chem. Lett.* **2016**, 7, 4438.
- [45] R. Österbacka, *Science* **2000**, 287, 839.
- [46] S. Kahmann, M. A. Loi, C. J. Brabec, *J. Mater. Chem. C* **2018**, 6, 6008.
- [47] N. Gasparini, A. García-Rodríguez, M. Prosa, Ş. Bayseç, A. Palma-Cando, A. Katsouras, A. Avgeropoulos, G. Pagona, V. G. Gregoriou, C. L. Chochos, S. Allard, U. Scherf, C. J. Brabec, T. Ameri, *Front. Energy Res.* **2017**, 4, 1.
- [48] L. Ke, N. Gasparini, J. Min, H. Zhang, M. Adam, S. Rechberger, K. Forberich, C. Zhang, E. Spiecker, R. R. Tykwinski, C. J. Brabec, T. Ameri, *J. Mater. Chem. A* **2017**, 5, 2550.
- [49] M. Salvador, N. Gasparini, J. D. Perea, S. H. Paleti, A. Distler, L. N. Inasaridze, P. A. Troshin, L. Luer, H.-J. Egelhaaf, C. Brabec, *Energy Environ. Sci.* **2017**, 10, 2005.
- [50] J. Niklas, K. L. Mardis, B. P. Banks, G. M. Grooms, A. Sperlich, V. Dyakonov, S. Beaupré, M. Leclerc, T. Xu, L. Yu, O. G. Poluektov, *Phys. Chem. Chem. Phys.* **2013**, 15, 9562.
- [51] N. Gasparini, A. Katsouras, M. I. Prodromidis, A. Avgeropoulos, D. Baran, M. Salvador, S. Fladischer, E. Spiecker, C. L. Chochos, T. Ameri, C. J. Brabec, *Adv. Funct. Mater.* **2015**, 25, 4898.
- [52] J. B. Gilroy, D. J. Lunn, S. K. Patra, G. R. Whittell, M. A. Winnik, I. Manners, *Macromolecules* **2012**, 45, 5806.
- [53] S. A. Dowland, M. Salvador, J. D. Perea, N. Gasparini, S. Langner, S. Rajoelson, H. H. Ramanitra, B. D. Lindner, A. Osvet, C. J. Brabec, R. C. Hiorns, H.-J. Egelhaaf, *ACS Appl. Mater. Interfaces* **2017**, 9, 10971.
- [54] J. D. Perea, S. Langner, M. Salvador, B. Sanchez-Lengeling, N. Li, C. Zhang, G. Jarvas, J. Kontos, A. Dallos, A. Aspuru-Guzik, C. J. Brabec, *J. Phys. Chem. C* **2017**, 121, 18153.
- [55] Y. Cui, C. Yang, H. Yao, J. Zhu, Y. Wang, G. Jia, F. Gao, J. Hou, *Adv. Mater.* **2017**, 29, 1703080.